Single production of an exotic vectorlike Y quark at future high energy pp colliders

Liangliang Shang,[1,2,*] Yuxiao Yan,[1,†] Stefano Moretti,[2,3,‡] and Bingfang Yang[1,§]

[1]*School of Physics, Henan Normal University, Xinxiang 453007, People's Republic of China*
[2]*Department of Physics and Astronomy, Uppsala University, Box 516, SE-751 20 Uppsala, Sweden*
[3]*School of Physics and Astronomy, University of Southampton, Highfield, Southampton SO17 1BJ, United Kingdom*

(Received 18 April 2024; accepted 10 May 2024; published 18 June 2024)

Vectorlike quarks have been predicted in various new physics scenarios beyond the Standard Model. In a simplified modelling of a (B, Y) doublet including a vectorlike quark Y, with charge $-\frac{4}{3}$e, there are only two free parameters: the Y coupling κ_Y and mass m_Y. In the five flavor scheme, we investigate the single production of the Y state decaying into Wb at the Large Hadron Collider (LHC) run-III and High-Luminosity LHC (HL-LHC) operating at $\sqrt{s} = 14$ TeV, the possible High-Energy LHC (HE-LHC) with $\sqrt{s} = 27$ TeV as well as the Future Circular Collider in hadron-hadron mode (FCC-hh) with $\sqrt{s} = 100$ TeV. Through detailed signal-to-background analyses and detector simulations, we assess the exclusion capabilities of the Y state at the different colliders. We find that this can be improved significantly with increasing collision energy, especially at the HE-LHC and FCC-hh, both demonstrating an obvious advantage with respect to the HL-LHC in the case of high m_Y. Assuming a 10% systematic uncertainty on the background event rate, the exclusion capabilities are summarized as follows: (1) the LHC run-III can exclude the correlated regions of $\kappa_Y \in [0.06, 0.5]$ and $m_Y \in [1500\ \text{GeV}, 3800\ \text{GeV}]$ with integrated luminosity $L = 300\ \text{fb}^{-1}$; (2) the HL-LHC can exclude the correlated regions of $\kappa_Y \in [0.05, 0.5]$ and $m_Y \in [1500\ \text{GeV}, 3970\ \text{GeV}]$ with $L = 3\ \text{ab}^{-1}$; (3) the HE-LHC can exclude the correlated regions of $\kappa_Y \in [0.06, 0.5]$ and $m_Y \in [1500\ \text{GeV}, 6090\ \text{GeV}]$ with $L = 3\ \text{ab}^{-1}$; (4) the FCC-hh can exclude the correlated regions of $\kappa_Y \in [0.08, 0.5]$ and $m_Y \in [1500\ \text{GeV}, 10080\ \text{GeV}]$ with $L = 3\ \text{ab}^{-1}$.

DOI: 10.1103/PhysRevD.109.115016

I. INTRODUCTION

In 2012, the ATLAS and CMS experiments at the Large Hadron Collider (LHC) made a significant discovery by confirming the existence of the Higgs boson, thereby providing further validation for the Standard Model (SM) [1,2]. However, the SM has certain limits in addressing several prominent issues, such as neutrino masses, gauge hierarchy, dark matter and dark energy. In various new physics scenarios like little Higgs models [3–6], extra dimensions [7], composite Higgs models [8–11], and other extended models [12–14], the vectorlike quarks (VLQs) are predicted to play a role in resolving the gauge hierarchy problem by mitigating the quadratic divergences of the Higgs field. Such VLQs are fermions with spin $\frac{1}{2}$ and possess the unique characteristic of undergoing both left- and right-handed component transformations under the electroweak (EW) symmetry group of the SM [15]. Unlike chiral quarks, VLQs do not acquire masses through Yukawa couplings to the Higgs field and therefore have the potential to counterbalance loop corrections to the Higgs boson mass stemming from the top quark of the SM. Furthermore, VLQs can generate characteristic signatures at colliders and have been widely studied (see, for example, [16–53]).

A VLQ model typically introduces four new states: T, B, X, and Y, their electric charges being $+\frac{2}{3}$, $-\frac{1}{3}$, $+\frac{5}{3}$, and $-\frac{4}{3}$, respectively. In such kind of model, VLQs can be categorized into three types: singlets (T), (B), doublets (X, T), (T, B), (B, Y), and triplets (X, T, B), (T, B, Y). The Y quark does not couple to a SM quark and a SM boson via renormalizable interactions as a singlet. However, it is expected to decay with a 100% branching ratio (BR) into a b quark and W boson when Y is lighter than the other VLQs, whether in a doublet or triplet.

In this study, we will focus on the observability of single Y production at the Large Hadron Collider (LHC) run-III, the High-Luminosity LHC (HL-LHC) [54,55], the High-Energy

*shangliangliang@htu.edu.cn, liangliang.shang@physics.uu.se
†yanyuxiao@stu.htu.edu.cn
‡s.moretti@soton.ac.uk, stefano.moretti@physics.uu.se
§yangbingfang@htu.edu.cn

LHC (HE-LHC) [56], and the Future Circular Collider operating in hadron-hadron mode (FCC-hh) [57], specifically, within the (B, Y) doublet realization.

The ATLAS collaboration conducted a search for single production of VLQ Y at 13 TeV with an integrated luminosity of 36.1 fb^{-1} [58]. They found that the upper limits on the mixing angle are as small as $|\sin\theta_R| = 0.17$ for a Y quark with a mass of 800 GeV in the (B, Y) doublet model, and $|\sin\theta_L| = 0.16$ for a Y quark with a mass of 800 GeV in the (T, B, Y) triplet model. The CMS collaboration also conducted a search for single production of Y states in the Wb channel at 13 TeV using 2.3 fb^{-1} of data [59]. They searched for final states involving one electron or muon, at least one b-tagged jet with large transverse momentum, at least one jet in the forward region of the detector plus (sizeable) missing transverse momentum. Their findings indicate that the observed (expected) lower mass limits are 1.40 (1.0) TeV for a VLQ Y with a coupling value of 0.5 and a $\mathrm{BR}(Y \to W^- b) = 1$. The ATLAS collaboration recently presented a search for the pair production of VLQ T in the lepton + jets final state using 140 fb^{-1} at 13 TeV [60]. They pointed out that the most stringent limits are set for the scenario $\mathrm{BR}(T \to W^+ b) = 1$, for which T masses below 1700 GeV (1570 GeV) are observed (expected) to be excluded at 95% confidence level (CL). And the limits can also apply to a VLQ Y with $\mathrm{BR}(Y \to W^- b) = 1$. All such limits stem from VLQ pair production, induced by quantum chromodynamics (QCD).

Furthermore, there are comparable exclusion limits on the mixing parameter $\sin\theta_R$ from EW precision observables (EWPOs), for example within the (B, Y) doublet model, Ref. [15] found that the upper limits on $\sin\theta_R$ are approximately 0.21 and 0.15 at $m_Y = 1000$ GeV and 2000 GeV respectively at 95% CL from the oblique parameters S and T. Reference [61] highlighted that, considering the W boson mass measurement by the CDF collaboration [62], the 2σ bounds on $\sin\theta_R$ from the oblique parameters S, T, and U are approximately [0.15, 0.23] and [0.09, 0.13] at $m_Y = 1000$ and 3000 GeV in a conservative average scenario, respectively. They also pointed out that the constraints from the $Zb\bar{b}$ coupling are weaker than those from the EWPOs for about $m_Y > 1600$ GeV.

The single production of a VLQ is instead model dependent, as the couplings involved are EW ones, yet they may make a significant contribution to the total VLQ production cross section, compared to the pair production, due to less phase space suppression, in the region of high VLQ masses. In this work, we will in particular focus on the process $pp \to Y(\to W^- b)j \to l^- \bar{\nu}_l b j$ in the five flavor scheme (with l^- standing for electron or muon and j standing for first two-generation quark jets), combined with its charged conjugated process $pp \to \bar{Y} j$. We expect that the forthcoming results will provide complementary information to the one provided by VLQ pair production in the quest to detect a doublet Y quark at the aforementioned future colliders.

The paper is structured as follows. In Sec. II, we introduce the simplified VLQ model used in our simulations. In Sec. III, we analyze the properties of the signal process and SM backgrounds. Subsequently, we conduct simulations and calculate the Y state exclusion and discovery capabilities at the HL-LHC, HE-LHC, and FCC-hh. Finally, in Sec. IV, we provide a summary.

II. DOUBLET VLQ Y IN A SIMPLIFIED MODEL

As mentioned, in a generic VLQ model, one can include four types of states called T, B, X, and Y, with electric charges $+\frac{2}{3}$, $-\frac{1}{3}$, $+\frac{5}{3}$, and $-\frac{4}{3}$, respectively. Under the SM gauge group, $SU(3)_C \times SU(2)_L \times U(1)_Y$, there are seven possible representations of VLQs as shown in Table I.

These representations allow for couplings between VLQs and SM gauge bosons and quarks. The kinetic and mass terms of the VLQs are described as [61]

$$\mathcal{L} = \sum_F \bar{F}(i\not{D} - M_F)F, \tag{1}$$

where $F = \{U, D, Q_1, Q_5, Q_7, T_1, T_2\}$, $D_\mu = \partial_\mu + ig_1 Y_F B_\mu + ig_2 S^I W^I_\mu + ig_s T^A G^A_\mu$, $\lambda^A (A = 1, 2, \ldots, 8)$, and $\tau^I (I = 1, 2, 3)$, related to the Gell-Mann and Pauli matrices via $T^A = \frac{1}{2}\lambda^A$ and $S^I = \frac{1}{2}\tau^I$, respectively. In our simplified model, we use an effective Lagrangian framework for the interactions of a VLQ Y with the SM quarks through W boson exchange, including as Y free parameters $\kappa_Y^{i,L/R}$ (couplings) and m_Y (mass) [63]:

$$\mathcal{L} = \left\{ \kappa_Y^{i,L/R} \sqrt{\frac{\zeta_i}{\Gamma_W^0}} \frac{g}{\sqrt{2}} [\bar{Y}_{L/R} W^-_\mu \gamma^\mu d^i_{L/R}] + \mathrm{H.c.} \right\} + m_Y \bar{Y} Y, \tag{2}$$

where $d^i_{L/R}$ represents the three SM generation quarks labeled by i, L, and R stand for the left-handed and right-handed chiralities, respectively, $\Gamma_W^0 = (1 - 3m_W^4/m_Y^4 + 2m_W^6/m_Y^6)$ for zero SM quark mass $m_q = 0$, and $\zeta_i = |V^{4i}_{L/R}|^2 / \sum_i |V^{4i}_{L/R}|^2$, $V^{4i}_{L/R}$ represents the mixing matrices

TABLE I. Representations of VLQs and their quantum numbers under the SM gauge group.

VLQ multiplet	U	D	Q_1	Q_5	Q_7	T_1	T_2
Component fields	T	B	(T, B)	(B, Y)	(X, T)	(T, B, Y)	(X, T, B)
$SU(3)_C$	3	3	3	3	3	3	3
$SU(2)_L$	1	1	2	2	2	3	3
$U(1)_Y$	2/3	−1/3	1/6	−5/6	7/6	−1/3	2/3

between the Y quark and the three SM generations. The current experimental constraints at the LHC tend to favor a Y quark mass at the TeV scale, leading to an approximate value of $\Gamma_W^0 = 1$. We assume that the Y only couples to the SM third generation quarks, that is, Y decays 100% into Wb and therefore $\zeta_1 = \zeta_2 = 0, \zeta_3 = 1$. Consequently, the above Lagrangian can be simplified as

$$\mathcal{L} = \left\{ \frac{g\kappa_Y^{3,L/R}}{\sqrt{2}} [\bar{Y}_{L/R} W_\mu^- \gamma^\mu b_{L/R}] + \text{H.c.} \right\} + m_Y \bar{Y} Y, \tag{3}$$

where g is the EW coupling constant. By comparing the Lagrangian for the (B, Y) doublet and (T, B, Y) triplet, we observe that the relationship between the coupling $\kappa_Y^{3,L/R}$ and mixing angle $\theta^{L/R}$ is $\sin\theta^{L/R} = \kappa_Y^{3,L/R}$ for the doublet and $\sin\theta^{L/R} = \sqrt{2}\kappa_Y^{3,L/R}$ for the triplet. Taking into account the relationships $\tan\theta^L = \frac{m_b}{m_B}\tan\theta^R$ and $\tan\theta^R = \frac{m_b}{m_B}\tan\theta^L$ as well as the condition $m_B \gg m_b$, we can assume $\kappa_Y^{3,L} = 0$ for the doublet and $\kappa_Y^{3,R} = 0$ for the triplet.[1] As mentioned in the introduction, Refs. [15,61] found that the upper limits on $\sin\theta_R$ are on the order of $\mathcal{O}(10^{-1})$ at 95% CL from the EWPOs. Therefore, a value smaller than 0.5 for κ_Y is considered in this study. The Y decay width can be expressed as [64]

$$\Gamma(Y \to Wq) = \frac{\alpha_e \kappa_Y^2}{16\sin^2\theta_W} \frac{(m_W^2 - m_Y^2)^2(2m_W^2 + m_Y^2)}{m_W^2 m_Y^3}, \tag{4}$$

where $\alpha_{\text{EM}} = \frac{g'^2}{4\pi}$, g' is the electromagnetic (EM) coupling constant and θ_W is the EW mixing angle. In this paper, we solely focus on the narrow width approximation (NWA), which we use for the purpose of simplifying scattering amplitude calculations. However, it is worth noting that several studies [31,40,65,66] have highlighted the limitations of the NWA in scenarios involving new physics with VLQs. Specifically, it becomes imperative to consider a finite width when this becomes larger than $\alpha_{\text{EM}} \approx 1\%$, given the substantial interference effects emerging between VLQ production and decay channels, coupled with their interactions with the corresponding irreducible backgrounds. To address the limitations of our approach then, we will also present the ratio Γ_Y/m_Y in our subsequent results and emphasize since now that, crucially, for the region where $\Gamma_Y/m_Y > 1\%$, our sensitivities may be under- or overestimated, as such interferences could be positive or negative, respectively. Besides, before starting with our numerical analysis, we remind the reader that one can apply the results of our forthcoming simulations to a specific VLQ representation, such as, e.g., (B, Y) or (T, B, Y), by utilizing the aforementioned relationships.

[1]In the subsequent content, we will use κ_Y to denote $\kappa_Y^{3,R}$ for the sake of simplicity.

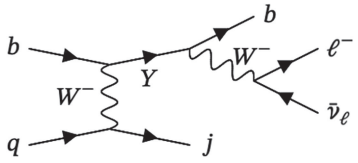

FIG. 1. Representative Feynman diagram of single Y production $pp \to Yj$ followed by its subsequent decay $Y \to W^-(\to l^-\bar{\nu}_l)b$ in the five flavor scheme. Here, q in the initial state represents one of the first two generation quarks, j in the final state represents one of the first two generation jets, b in the initial (final) state represents a b-quark (jet) while l^- represents either an electron or muon.

There are stringent limits from the oblique parameters S, T, and U from the EWPOs [15,61,67–77]. These oblique parameters relate to weak isospin currents and EM currents, involving their vacuum polarization amplitudes. Consequently, the oblique parameters can be reformulated using the vacuum polarizations of the SM gauge bosons. The contributions in the doublet (B, Y) model to these oblique parameters can be approximated as follows [61]:

$$S \simeq \frac{1}{2\pi}\left\{ -\frac{2}{3}\kappa_Y^2 \ln\frac{\mathcal{M}^2}{m_b^2} + \frac{11}{3}\kappa_Y^2 \right\}, \quad U \simeq -\frac{\kappa_Y^2}{2\pi},$$
$$T \simeq \frac{3m_t^2}{8\pi\sin^2\theta_W m_W^2}\kappa_Y^4 \frac{2\mathcal{M}^2}{3m_t^2}. \tag{5}$$

Here, $\mathcal{M}^2 = (m_Y^2 - m_b^2\kappa_Y^2)/(1-\kappa_Y^2)$ and $m_W = m_Z\cos\theta_W$. For the numerical calculation, the χ^2 function for the oblique parameter fit should be less than 8.02 for three degrees of freedom to compute the 2σ limits, yielding: $S = -0.02 \pm 0.1$, $T = 0.03 \pm 0.12$, $U = 0.01 \pm 0.11$. Note that there exists a strong correlation of 92% between the S and T parameters while the U parameter exhibits an anticorrelation of $-80\%(-93\%)$ with S (T) [78]. Specific numerical values of the input parameters are detailed in Eq. (6).

In Fig. 1, we show a representative Feynman diagram of the signal production $pp \to Yj$ and decay chain $Y \to W^-(\to l^-\bar{\nu}_l)b$. We expect the W boson and the high-momentum b-jet to exhibit a back-to-back alignment in the transverse plane, originating from the decay of the massive Y quark. The topology also encompasses an outgoing light quark, often resulting in a forward jet within the detector. According to these features of signal events, the primary SM backgrounds include $pp \to t(\to l^+ b\nu_l)j$, $pp \to W^\pm(\to l\nu_l)bj$, $pp \to W^\pm(\to l\nu_l)W^\mp(\to jj)b$ plus their charge conjugated processes. Amongst these, the first two are irreducible backgrounds while the last one is a reducible background. We have also assessed additional backgrounds, such as $pp \to t\bar{t}$ and $pp \to Zbj$, and found that their contributions can be ignored based on the selection criteria that will be discussed later.

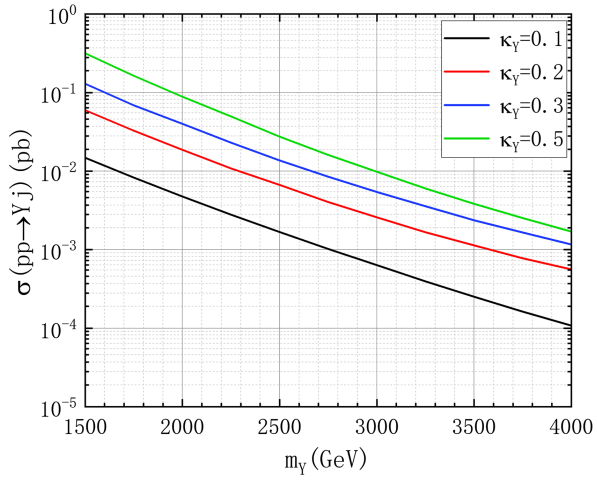

FIG. 2. The tree-level cross sections for single Y production $pp \to Y(\to W^- b)j$ as a function of the mass m_Y for various values of the coupling κ_Y. The charge conjugated process has also been included.

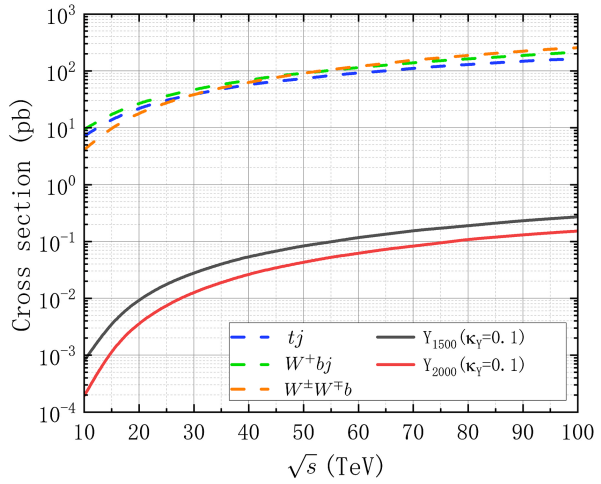

FIG. 3. The tree-level cross sections as a function of the center-of-mass energy $\sqrt{s}$ for the signal benchmarks and backgrounds. Solid lines represent the signal processes $pp \to Y(\to l^- \bar{\nu}_l b)j$ and dashed lines represent the background processes $pp \to t(\to l^+ b\nu_l)j$, $pp \to W^\pm(\to l\nu_l)bj$, $pp \to W^\pm(\to l\nu_l)W^\mp(\to jj)b$. The cross sections also include the charge conjugated processes.

The signal production cross section is determined not only by the mass m_Y but also by the coupling strength κ_Y. The cross section is directly proportional to κ_Y^2 for a fixed m_Y as long as the NWA is met [66]. In Fig. 2, we show the tree-level cross sections for single Y production as a function of the mass m_Y. We can see that, as m_Y increases, the cross section gradually decreases. Actually, this is mostly attributed to the fact that the gluon parton distribution function grow smaller at the larger x values needed to produce the ever more massive final state.

In Fig. 3, we show the tree-level cross sections for the signal benchmarks $m_Y = 1500$ GeV (labeled as Y_{1500}) and $m_Y = 2000$ GeV (labeled as Y_{2000}) with $\kappa_Y = 0.1$ as well as the tree-level cross sections for the background processes. The signal cross sections for different values of κ_Y can be obtained by rescaling. It is evident that the rates for the backgrounds are significantly larger than those for the signals. Consequently, we should design efficient selection criteria in terms of kinematic cuts to reduce the number of background events while preserving the signal events. Furthermore, the cross sections for both signal and backgrounds increase with increasing collider energy.

TABLE II. K factors representing the QCD corrections for the background processes.

Processes	tj	$W^\pm bj$	$W^\pm W^\mp b$
K factor	1.1 [79–81]	1.9 [82]	2.1 [82]

The next-to-leading order or even higher order QCD corrections for the SM background cross sections at the LHC have been extensively explored in Refs. [79–82]. The K factors associated with the background cross sections adopted in our calculations are summarized in Table II.[2]

III. SIGNAL TO BACKGROUND ANALYSIS

The signal model file is sourced from FeynRules [84] and parton-level events are generated using MadGraph5_aMC@NLO [85] with the parton distribution function of NNPDF23LO1 [86]. Dynamic factorization and renormalization scales are set as default in MadEvent [87]. Subsequently, fast detector simulations are conducted using DELPHES 3.4.2 [88] with the built-in detector configurations of the LHC run-III, HL-LHC, HE-LHC [89], and FCC-hh [90]. Jets are clustered by FastJet [91] employing the anti-kt algorithm [92] with a distance parameter of $\Delta R = 0.4$. Furthermore, MadAnalysis 5 [93] is used to analyze both signal and background events. Finally, the EasyScan_HEP package [94] is utilized to connect these programs and scan the VLQ parameter space.

The numerical values of the input SM parameters are taken as follows [78]:

$$\begin{aligned} &m_b = 4.18 \text{ GeV}, \qquad m_t = 172.69 \text{ GeV}, \\ &m_Z = 91.1876 \text{ GeV}, \qquad \sin^2\theta_W = 0.22339, \\ &\alpha(m_Z) = 1/127.951, \qquad \alpha_s(m_Z) = 0.1179. \end{aligned} \tag{6}$$

Considering the general detection capabilities of detectors, the following basic cuts at the parton level are chosen[3]:

[2]Note that, despite they change somewhat with energy, we neglect here the changes of K factors values at different colliders, like in Ref. [83].

[3]Note that $\Delta R > 0.4$ is required as part of the parton-level settings in run_card.dat of MadGraph5_aMC@NLO. This requirement is implemented to enhance the percentage of events generated at the parton level that satisfy the criteria for isolated particles. For events involving isolated particles in MadAnalysis 5, we similarly impose $\Delta R > 0.4$ at the detector simulation level in delphes_card.dat, following the default requirement in DELPHES.

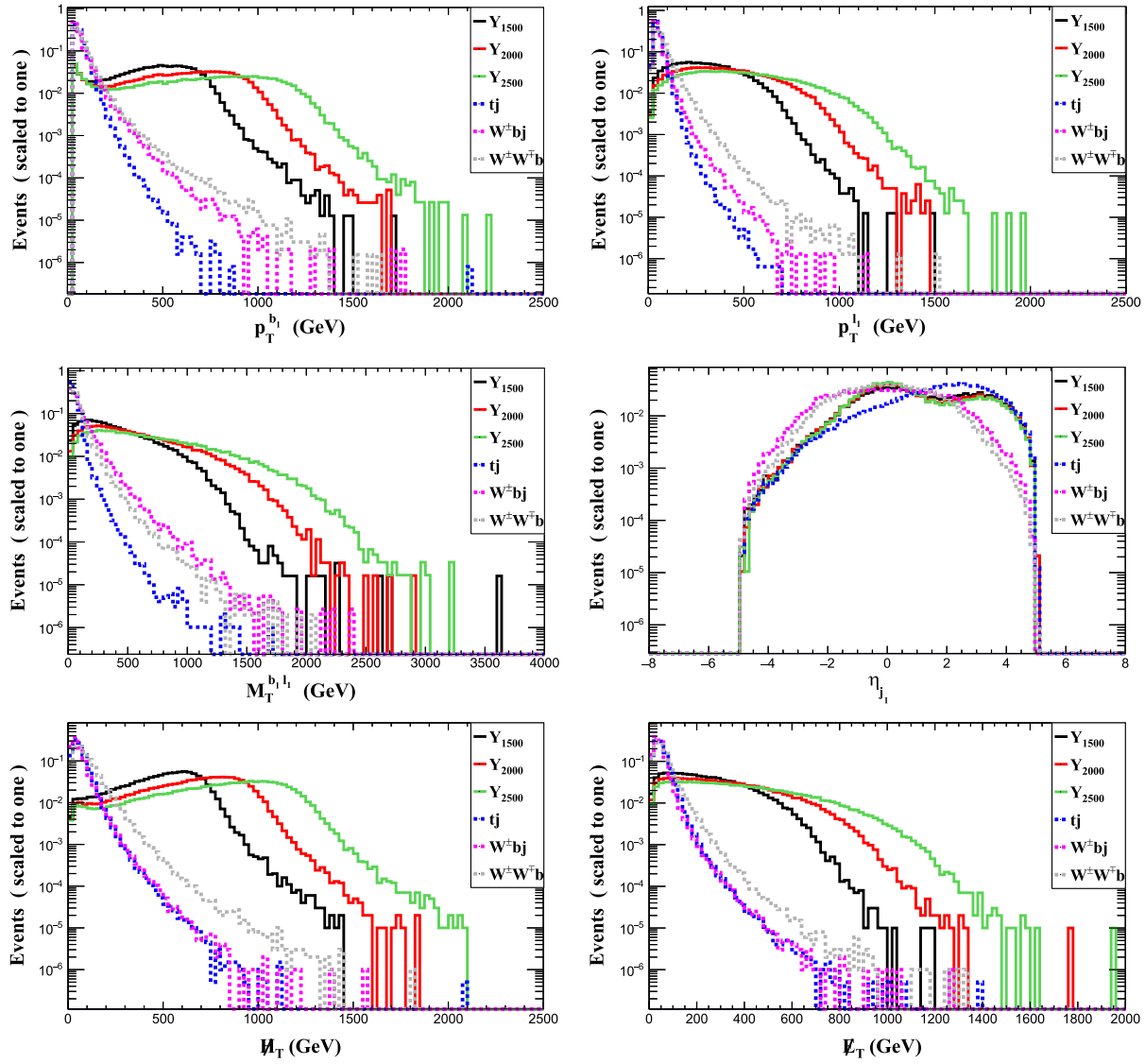

FIG. 4. Normalized distributions for the signals of $m_Y = 1500$, 2000, and 2500 GeV and SM backgrounds at the HL-LHC. The conjugated processes have been included.

$$\Delta R(x,y) > 0.4 \quad (x,y = l,j,b), \quad p_T^l > 25\,\text{GeV}, \quad |\eta_l| < 2.5, \quad p_T^j > 20\,\text{GeV}, \quad |\eta_j| < 5.0, \quad p_T^b > 25\,\text{GeV}, \quad |\eta_b| < 2.5,$$

where $\Delta R = \sqrt{\Delta\Phi^2 + \Delta\eta^2}$ denotes the separation in the rapidity(η)-azimuth(ϕ) plane.

To handle the relatively small event number of signal (s) and background (b) events, we will use the median significance $\mathcal{Z}$ to estimate the expected discovery and exclusion reaches [95,96],

TABLE III. Cut flows of the signal with $\kappa_Y = 0.1$ and backgrounds at the 14 TeV HL-LHC, where the conjugate processes $pp \to \bar{t}j$, $W^{\mp}\bar{b}j$, $W^{\mp}W^{\pm}\bar{b}$ have been included.

Cuts	Y_{1500} (fb)	Y_{2000} (fb)	Y_{2500} (fb)	tj (fb)	$W^{\pm}bj$ (fb)	$W^{\pm}W^{\mp}b$ (fb)
Basic cuts	3.06	0.98	0.35	14117	30001	18967
Cut 1	1.70	0.54	0.19	5 774	8380	8635
Cut 2	0.83	0.32	0.12	0.07	5.85	12.61
Cut 3	0.51	0.25	0.10	0.03	3.18	7.08
Cut 4	0.28	0.13	0.05	0.01	0.21	0.48
Cut 5	0.24	0.12	0.05	0.01	0.09	0.27

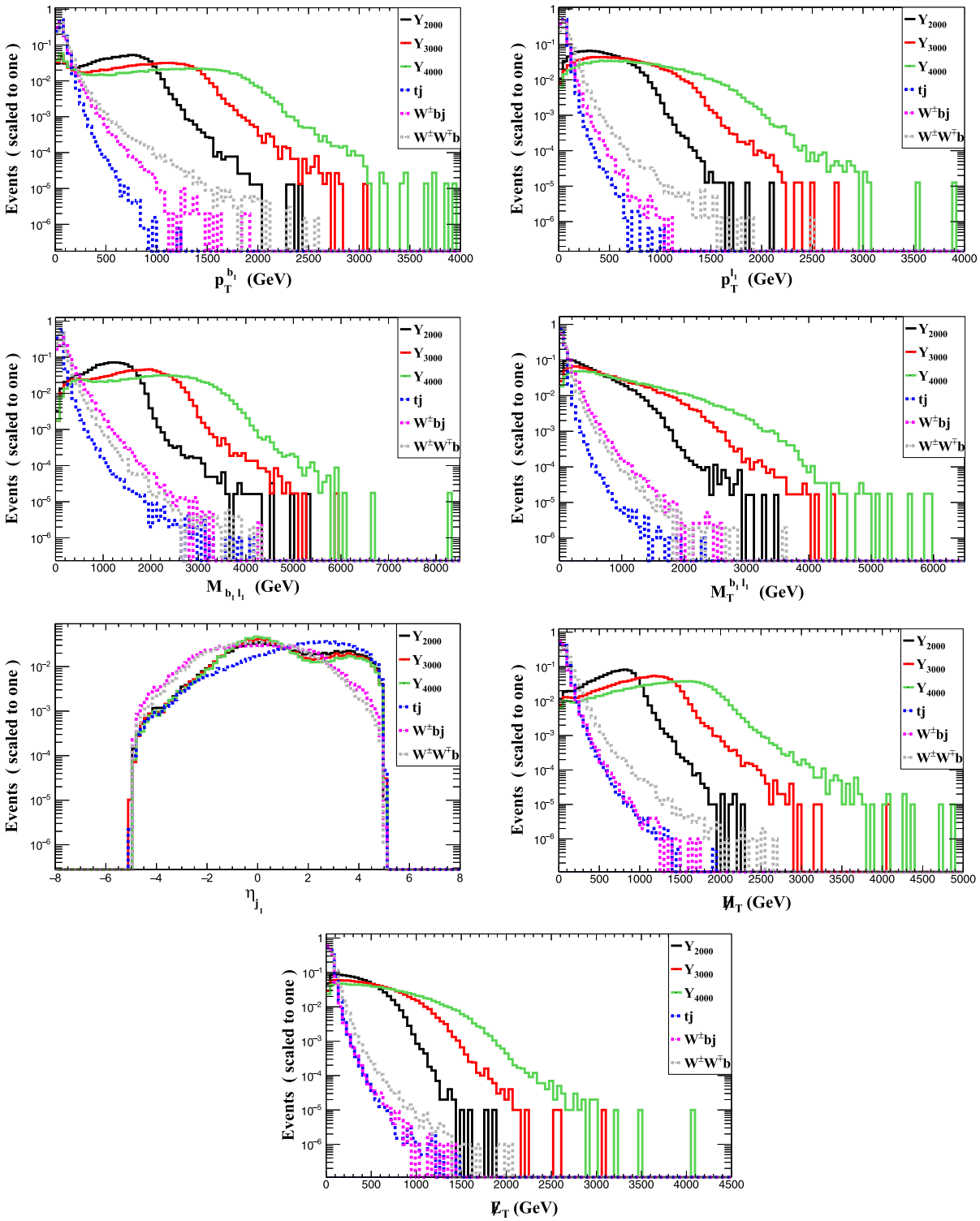

FIG. 5. Normalized distributions for the signals with $m_Y = 2000$, 3000, and 4000 GeV and backgrounds at the HE-LHC.

$$\mathcal{Z}_{\text{excl}} = \sqrt{2\left[s - b\ln\left(\frac{b+s+x}{2b}\right) - \frac{1}{\delta^2}\ln\left(\frac{b-s+x}{2b}\right)\right] - (b+s-x)\left(1+\frac{1}{\delta^2 b}\right)}, \tag{7}$$

$$\mathcal{Z}_{\text{disc}} = \sqrt{2\left[(s+b)\ln\left(\frac{(s+b)(1+\delta^2 b)}{b+(s+b)\delta^2 b}\right) - \frac{1}{\delta^2}\ln\left(1+\frac{\delta^2 s}{1+\delta^2 b}\right)\right]}, \tag{8}$$

TABLE IV. Cut flows of the signal with $\kappa_Y = 0.1$ and backgrounds at the 27 TeV HE-LHC.

Cuts	Y_{2000} (fb)	Y_{3000} (fb)	Y_{4000} (fb)	tj (fb)	$W^{\pm}bj$ (fb)	$W^{\pm}W^{\mp}b$ (fb)
Basic cuts	9.59	2.41	0.73	37406	77274	69303
Cut 1	5.34	1.29	0.38	15814	23225	32315
Cut 2	3.03	0.86	0.26	0.56	26	94.74
Cut 3	2.69	0.83	0.25	0.15	11.60	25.09
Cut 4	2.07	0.74	0.24	0.07	8.19	17.88
Cut 5	1.05	0.34	0.10	0.04	0.39	1.87
Cut 6	0.91	0.31	0.09	0.04	0.08	1.11

$$x = \sqrt{(s+b)^2 - \frac{4\delta^2 s b^2}{1+\delta^2 b}}, \tag{9}$$

where δ is the uncertainty that inevitably appears in the measurement of the background. The exclusion capability corresponds to $\mathcal{Z}_{\rm excl} = 2$ while the discovery potential corresponds to $\mathcal{Z}_{\rm disc} = 5$. In the completely ideal case, that is $\delta = 0$, Eqs. (7) and (8) can be simplified as follows:

$$\mathcal{Z}_{\rm excl} = \sqrt{2\left[s - b\ln\left(1+\frac{s}{b}\right)\right]}, \tag{10}$$

and

$$\mathcal{Z}_{\rm disc} = \sqrt{2\left[(s+b)\ln\left(1+\frac{s}{b}\right) - s\right]}. \tag{11}$$

A. LHC run-III and HL-LHC

Firstly, we establish a selection that emulates the LHC run-III and HL-LHC detector response based on the count of final state particles detected in each event. Given the limited efficiency of the detector in identifying jets, we adopt a lenient approach towards the number of jets. Consequently, the final count selection is defined as follows: $N_l = 1$, $N_b \geq 1$, $N_j \geq 1$.

Considering that the mass of Y is notably greater than that of its decay products, the latter exhibit distinct spatial characteristics in pseudorapidity η and spatial separation ΔR compared to backgrounds. These differences inform our selection criteria.

Furthermore, since the mass range of Y is much heavier than the particles originating from background processes, we anticipate that the transverse momentum (referred to as $\vec{p}_T$ and its magnitude denoted as p_T) of decay products of the Y state will be substantially larger than those of the same particles from the background processes. Besides, we will also consider variables such as $\not{E}_T$, $\not{H}_T$, $M_T(b_1, l_1)$, $M(b_1, l_1)$, and $M(b_1, l_1, j_1)$ to distinguish the signal from the background. Here, $\not{E}_T$ is missing energy representing the magnitude of the sum of the transverse momenta of all visible final state particles, $\not{H}_T$ is analogous to $\not{E}_T$ but only considers all visible hadronic momenta, M is reconstructed mass by energy-momentum of specific final states, while the transverse mass M_T is defined as follows:

$$\begin{aligned} M_T^2 &\equiv [E_T(1) + E_T(2)]^2 - [\vec{p}_T(1) + \vec{p}_T(2)]^2, \\ &= m_1^2 + m_2^2 + 2[E_T(1)E_T(2) - \vec{p}_T(1)\cdot\vec{p}_T(2)], \end{aligned}$$

where $E_T(i) = \sqrt{p_T^2(i) + m_i^2}$ and $m_i^2 = p_i^2$ with p_i representing a four vector.

In Fig. 4, we present the normalized distributions of $p_T^{b_1}$, $p_T^{l_1}$, $M_T^{b_1 l_1}$, η_{j_1}, $\not{H}_T$, and $\not{E}_T$ for $m_Y = 1500$ GeV, $m_Y = 2000$ GeV, and $m_Y = 2500$ GeV with $\kappa_Y = 0.1$ as well as for the background processes. Based on these distributions, we have devised the following selection criteria to distinguish the signal from the various backgrounds[4]:

(1) Cut-1: $N_l = 1$, $N_b \geq 1$, $N_j \geq 1$.
(2) Cut-2: $p_T^{b_1} > 350$ GeV and $p_T^{l_1} > 200$ GeV.
(3) Cut-3: $M_T^{b_1 l_1} > 300$ GeV.
(4) Cut-4: $\eta_{j_1} > 1.8$.
(5) Cut-5: $\not{H}_T > 300$ GeV and $\not{E}_T > 100$ GeV.

By applying these cuts, we can see that the signal efficiencies for $m_Y = 1500$ GeV, $m_Y = 2000$ GeV, and $m_Y = 2500$ GeV are approximately 8%, 12%, and 13%, respectively. The higher efficiency for the latter can be attributed to the larger transverse boost of the final state originating from an heavier Y. Meanwhile, the background processes are significantly suppressed. For reference, we provide the cut flows in Table III.

We present the exclusion capability ($\mathcal{Z}_{\rm excl} = 2$) and discovery potential ($\mathcal{Z}_{\rm disc} = 5$) for Y with two different integrated luminosities, 1000 fb^{-1} and 3000 fb^{-1}, at the HL-LHC, as shown in the top line of Fig. 7. In detail, we commence the calculation from $m_Y = 1500$ GeV up to 4000 GeV and select benchmark points at intervals of 250 GeV with $\kappa_Y = 0.1$ to obtain their cross sections (σ_s) and efficiencies (ϵ_s) for the process $pp \to Yj \to W^-(\to l^-\bar{\nu}_l)bj$. For each signal benchmark, we generate 10^5 events, and for each background, we generate 10^6 events. We have verified that different values of κ_Y yield the

[4]The subscript on the particle symbol is arranged according to the magnitude of the particle transverse momentum: e.g., in the case of b-jets, $p_T^{b_1}$ is greater than $p_T^{b_2}$.

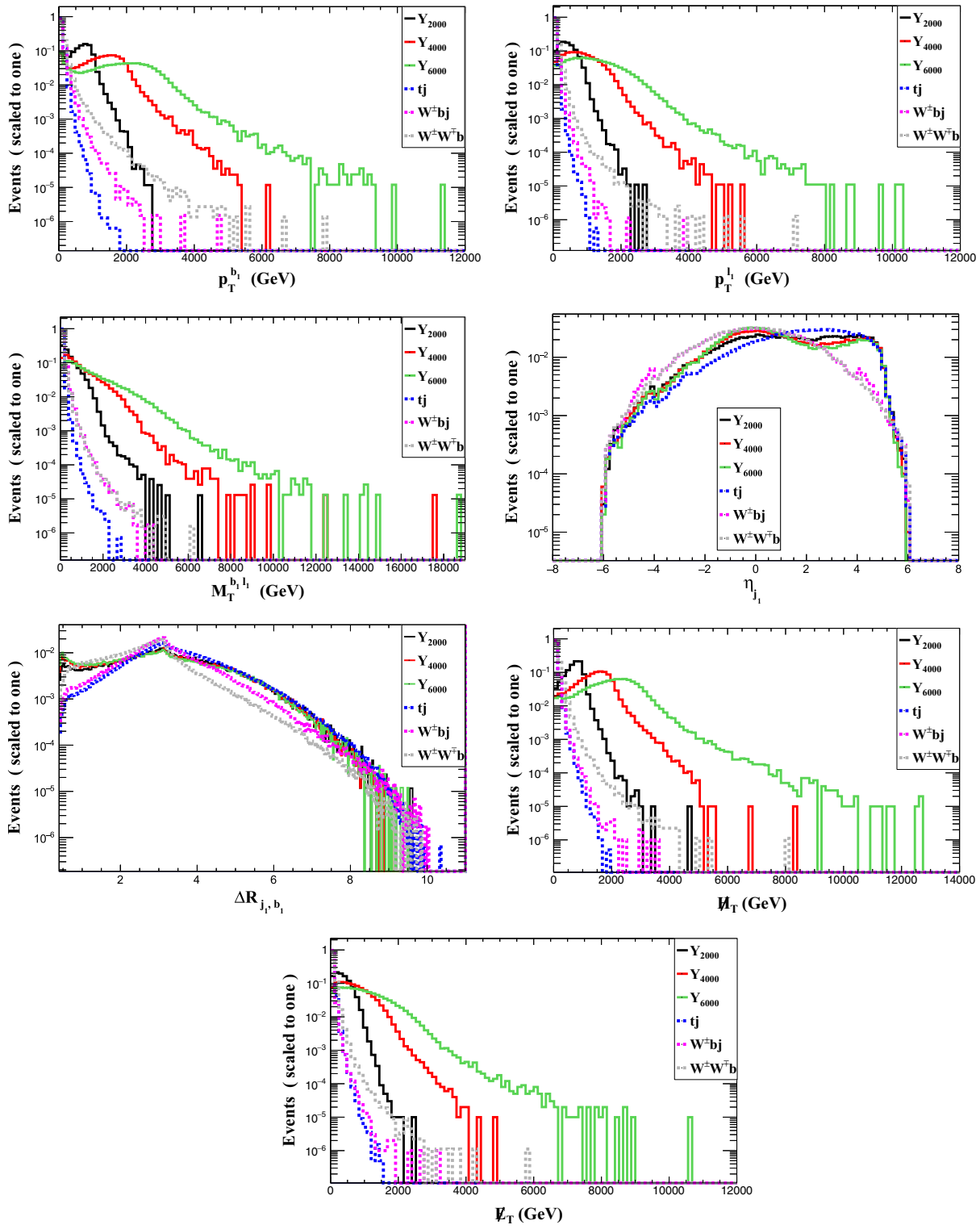

FIG. 6. Normalized distributions for the signals with $m_Y = 2000$, 4000, and 6000 GeV, and backgrounds at the FCC-hh.

same efficiency when m_Y remains constant. Furthermore, as illustrated in Fig. 1, the cross section σ_s is approximately proportional to the square of κ_Y. Consequently, we can set $s \approx L \times \sigma_s/(0.1)^2 \times \kappa_Y^2 \times \epsilon_s$ in Eqs. (7) and (8). Thus, for a specific integrated luminosity (L), we can determine the corresponding κ_Y value when Y is discovered or excluded. We consider both the ideal scenario without systematic uncertainties and the case with a 10% systematic uncertainty. In the presence of 10% systematic uncertainty, the Y can be excluded in the correlated parameter space

TABLE V. Cut flows of the signal with $\kappa_Y = 0.1$ and backgrounds at the 100 TeV FCC-hh.

Cuts	Y_{2000} (fb)	Y_{4000} (fb)	Y_{6000} (fb)	tj (fb)	$W^{\pm}bj$ (fb)	$W^{\pm}W^{\mp}b$ (fb)
Basic cuts	155.58	30.65	9.06	182592	411730	573258
Cut 1	90.71	17.48	5.09	90355	163348	299942
Cut 2	33.82	12.18	3.77	1.19	76.17	580
Cut 3	25.3	10.87	3.56	1.0	67.11	481
Cut 4	10.90	4.02	1.22	0.27	3.29	49.82
Cut 5	9.52	3.43	1.04	0.27	2.90	35.77
Cut 6	8.35	3.21	0.99	0.09	0.82	16

of $\kappa_Y \in [0.06, 0.5]$ and $m_Y \in [1500\ \text{GeV}, 3800\ \text{GeV}]$ with an integrated luminosity of $L = 300\ \text{fb}^{-1}$, which corresponds to the maximum achievable integrated luminosity during LHC run-III. If the integrated luminosity is raised to $3000\ \text{fb}^{-1}$, aligning with the maximum achievable at the HL-LHC, then the excluded parameter space extends to $\kappa_Y \in [0.05, 0.5]$ and $m_Y \in [1500\ \text{GeV}, 3970\ \text{GeV}]$.

B. 27 TeV HE-LHC

This section delves into the prospective signal of Y at the future 27 TeV HE-LHC. We commence the calculation from $m_Y = 1500$ GeV up to 7000 GeV and select benchmark points at intervals of 250 GeV with $\kappa_Y = 0.1$. In Fig. 5, we exhibit the normalized distributions for signal of $m_Y = 2000$, 3000, and 4000 GeV as well as background processes, forming the basis for our distinctive selection criteria:

(1) Cut-1: $N_l = 1$, $N_b \geq 1$, $N_j \geq 1$.
(2) Cut-2: $p_T^{b_1} > 300$ GeV and $p_T^{l_1} > 250$ GeV.
(3) Cut-3: $M_{b_1 l_1} > 1000$ GeV.
(4) Cut-4: $M_T^{b_1 l_1} > 200$ GeV.
(5) Cut-5: $\eta_{j_1} > 2.0$.
(6) Cut-6: $\not{H}_T > 400$ GeV and $\not{E}_T > 100$ GeV.

The kinematic variables compared to the 14 TeV case, an additional variable $M_{b_1 l_1}$ is introduced here. The cut threshold values for transverse momentum-based variables, such as $\not{H}_T > 400$ GeV, are higher than those in the 14 TeV case. This adjustment accounts for the increased center-of-mass energy. Detailed cut flows are outlined in Table IV and the exclusion capability and discovery potential are shown in the second row of Fig. 7. The signal efficiencies for $m_Y = 2000$ GeV, $m_Y = 3000$ GeV, and $m_Y = 4000$ GeV are approximately 9%, 13%, and 13%, respectively. The Y quark can be excluded within the correlated parameter space of $\kappa_Y \in [0.06, 0.5]$ and $m_Y \in [1500\ \text{GeV}, 6090\ \text{GeV}]$ with 10% systematic uncertainty for $L = 10\ \text{ab}^{-1}$. We note that the loss of sensitivity at low masses as being due to the cuts being optimised for heavy masses.

C. 100 TeV FCC-hh

Here, we explore the anticipated signal of Y in the context of the future 100 TeV FCC-hh. We commence the calculation from $m_Y = 1500$ GeV up to 15000 GeV and select benchmark points at intervals of 250 GeV with $\kappa_Y = 0.1$. The figures in Fig. 6 portray normalized distributions for signal of $m_Y = 2000$, 4000, and 6000 GeV as well as and background processes, laying the groundwork for our distinctive selection criteria:

(1) Cut-1: $N_l = 1$, $N_b \geq 1$, $N_j \geq 1$.
(2) Cut-2: $p_T^{b_1} > 700$ GeV and $p_T^{l_1} > 220$ GeV.
(3) Cut-3: $M_T^{b_1 l_1} > 200$ GeV.
(4) Cut-4: $2.4 < \eta_{j_1} < 4.8$.
(5) Cut-5: $\Delta R_{j_1 b_1} > 3.0$.
(6) Cut-6: $\not{H}_T > 400$ GeV and $\not{E}_T > 150$ GeV.

Compared to the 14 TeV case, an additional variable $\Delta R_{j_1 b_1}$ is introduced here. Upon analyzing the distributions of $\Delta R_{j_1 b_1}$, it is apparent that the signal tends to be more central than the backgrounds. Thus, we require $\Delta R_{j_1 b_1} > 3.0$. The signal efficiencies for $m_Y = 2000$ GeV, $m_Y = 4000$ GeV, and $m_Y = 6000$ GeV are approximately 5%, 10%, and 11%, respectively. Notably, there is a significant suppression in the background processes. Comprehensive cut flows are provided in Table V. The exclusion capability and discovery potential are illustrated in the final row of Fig. 7. It is evident that the systematic uncertainty has a considerable impact on the results. Even with a 10% systematic uncertainty, the parameter space will significantly shrink. Accounting for the 10% systematic uncertainty, the Y quark can be excluded within the correlated parameter space of $\kappa_Y \in [0.08, 0.5]$ and $m_Y \in [1500\ \text{GeV}, 10080\ \text{GeV}]$ at the highest design value of luminosity, $L = 30\ \text{ab}^{-1}$.

IV. SUMMARY

In a simplified model, we have investigated the single production of a doublet VLQ denoted by Y in the Wb decay channel at the $\sqrt{s} = 14$ TeV HL-LHC, $\sqrt{s} = 27$ TeV HE-LHC and $\sqrt{s} = 100$ TeV FCC-hh, following its production via $pp \to Yj$, with the W decaying into electrons and muons plus their respective neutrinos. We have performed a detector level simulation for the signal and relevant SM backgrounds. Considering a systematic uncertainty of 10% with an integrated luminosity of $3000\ \text{fb}^{-1}$, we describe the exclusion and discovery capabilities as follows: (1) The HL-LHC can exclude (discover) the region of $\kappa_Y \in [0.05, 0.5]$ ($[0.09, 0.5]$) and $m_Y \in [1500\ \text{GeV}, 3970\ \text{GeV}]$ ($[1500\ \text{GeV},$

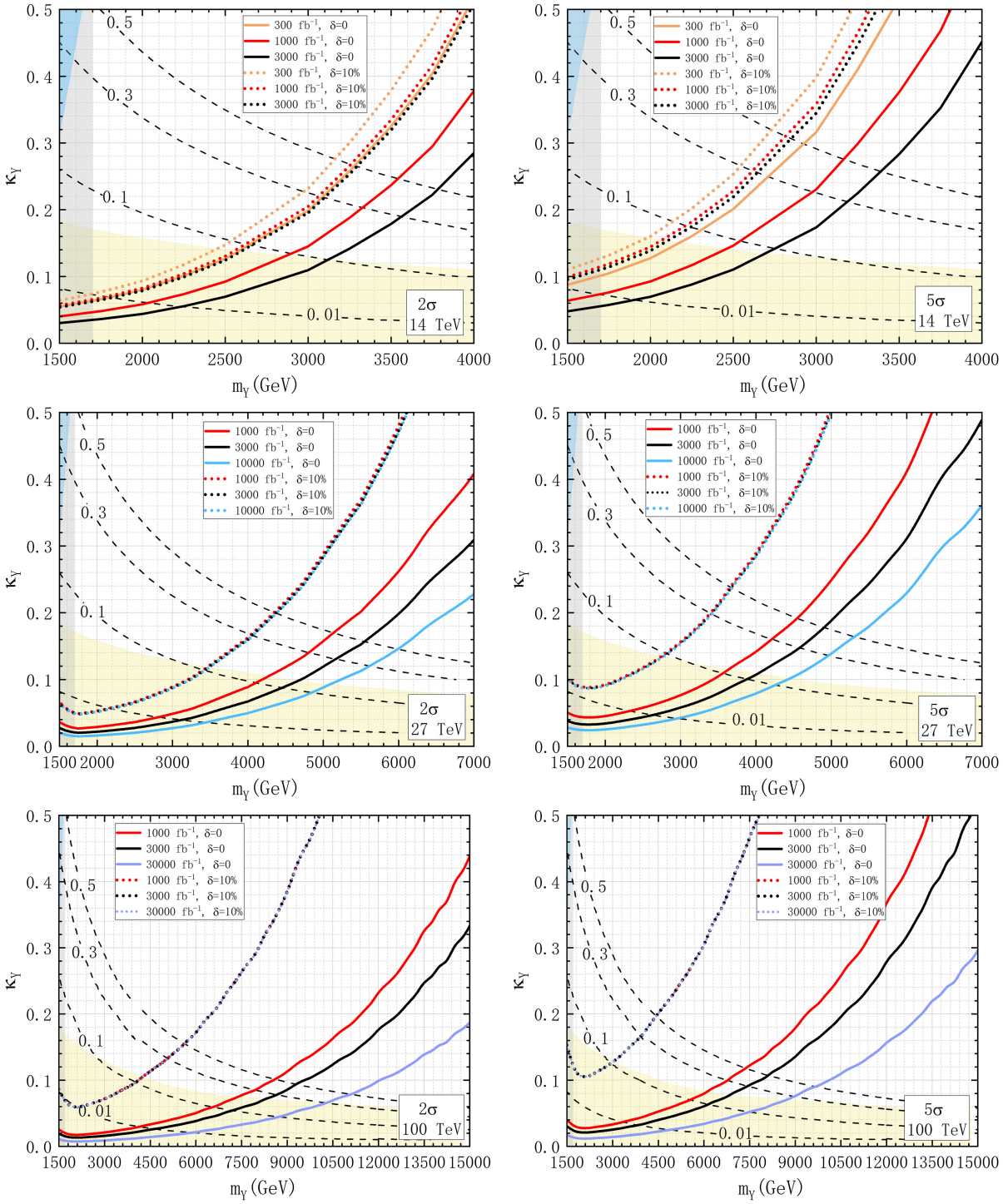

FIG. 7. The exclusion capability ($\mathcal{Z}_{\rm excl} = 2$) and discovery potential ($\mathcal{Z}_{\rm disc} = 5$) for the Y state at the LHC run-III and HL-LHC, $\sqrt{s} = 27$ TeV HE-LHC and $\sqrt{s} = 100$ TeV FCC-hh. Solid lines represent the ideal scenario without systematic uncertainty, the dotted lines represent the scenario with a 10% systematic uncertainty. Dashed lines denote the contours of Γ_Y/m_Y. The blue (gray) shaded area indicates the exclusion region of the current LHC at $\sqrt{s} = 13$ TeV with $L = 36.1$ fb^{-1} (140 fb^{-1}), as reported in Ref. [58] (Ref. [60]). Meanwhile, the yellow shaded area denotes the allowed region for the oblique parameters S, T, and U, considering the current measurements in Ref. [78].

3360 GeV]). (2) The HE-LHC can exclude (discover) the region of $\kappa_Y \in [0.06, 0.5]$ ($[0.1, 0.5]$) and $m_Y \in [1500\ \text{GeV}, 6090\ \text{GeV}]$ ($[1500\ \text{GeV}, 5000\ \text{GeV}]$). (3) The FCC-hh can exclude (discover) the region of $\kappa_Y \in [0.08, 0.5]$ ($[0.14, 0.5]$) and $m_Y \in [1500\,\text{GeV}, 10080\,\text{GeV}]$ ($[1500\ \text{GeV}, 7800\ \text{GeV}]$). All information of Y exclusion and discovery can be clearly seen in Fig. 7.

If the mass of Y is notably greater than that of its decay products and much heavier than the particles originating from background processes, then the signal exhibits more distinct characteristics compared to backgrounds. However, as the mass of Y increases, the cross section of the signal decreases. Therefore, there is a balance between these two aspects, and we observe an optimal discovery reach depicted as a curve bulge in Fig. 7.

Furthermore, we highlight that the stringent constraint on the VLQ Y, derived from the Y pair production search with $\text{BR}(Y \to W^- b) = 1$, imposes $m_Y > 1700$ GeV. In this context, we reassess the potential of LHC run-III to explore the VLQ Y, revealing that the associated parameter regions of $\kappa_Y \in [0.06, 0.5]$ ($[0.11, 0.5]$) and $m_Y \in [1500\ \text{GeV}, 3800\ \text{GeV}]$ ($[1500\ \text{GeV}, 3200\ \text{GeV}]$) can be excluded (discovered) based on LHC run-III luminosity. We foresee that our investigation will spur complementary explorations for a potential Y quark at forthcoming pp colliders.

ACKNOWLEDGMENTS

This work of L. S., Y. Y., and B. Y. is supported by the Natural Science Foundation of Henan Province under Grant No. 232300421217, the National Research Project Cultivation Foundation of Henan Normal University under Grant No. 2021PL10, the China Scholarship Council under Grant No. 202208410277 and also powered by the High Performance Computing Center of Henan Normal University. The work of S. M. is supported in part through the NExT Institute, the Knut and Alice Wallenberg Foundation under the Grant No. KAW 2017.0100 (SHIFT) and the STFC Consolidated Grant No. ST/L000296/1.

[1] G. Aad *et al.* (ATLAS Collaboration), Observation of a new particle in the search for the standard model Higgs boson with the ATLAS detector at the LHC, Phys. Lett. B **716**, 1 (2012).
[2] S. Chatrchyan *et al.* (CMS Collaboration), Observation of a new boson at a mass of 125 GeV with the CMS experiment at the LHC, Phys. Lett. B **716**, 30 (2012).
[3] N. Arkani-Hamed, A. G. Cohen, E. Katz, and A. E. Nelson, The littlest Higgs, J. High Energy Phys. 07 (2002) 034.
[4] T. Han, H. E. Logan, B. McElrath, and L.-T. Wang, Phenomenology of the little Higgs model, Phys. Rev. D **67**, 095004 (2003).
[5] S. Chang and H.-J. He, Unitarity of little Higgs models signals new physics of UV completion, Phys. Lett. B **586**, 95 (2004).
[6] Q.-H. Cao and C.-R. Chen, Signatures of extra gauge bosons in the littlest Higgs model with T-parity at future colliders, Phys. Rev. D **76**, 075007 (2007).
[7] K. Agashe, G. Perez, and A. Soni, Collider signals of top quark flavor violation from a warped extra dimension, Phys. Rev. D **75**, 015002 (2007).
[8] K. Agashe, R. Contino, and A. Pomarol, The minimal composite Higgs model, Nucl. Phys. **B719**, 165 (2005).
[9] B. Bellazzini, C. Csáki, and J. Serra, Composite Higgses, Eur. Phys. J. C **74**, 2766 (2014).
[10] M. Low, A. Tesi, and L.-T. Wang, Twin Higgs mechanism and a composite Higgs boson, Phys. Rev. D **91**, 095012 (2015),
[11] L. Bian, D. Liu, and J. Shu, Low scale composite Higgs model and 1.8–2 TeV diboson excess, Int. J. Mod. Phys. A **33**, 1841007 (2018).
[12] H.-J. He, T. M. P. Tait, and C. P. Yuan, New top flavor models with a seesaw mechanism, Phys. Rev. D **62**, 011702 (2000).
[13] X.-F. Wang, C. Du, and H.-J. He, LHC Higgs signatures from topflavor seesaw mechanism, Phys. Lett. B **723**, 314 (2013).
[14] H.-J. He, C. T. Hill, and T. M. P. Tait, Top quark seesaw model, vacuum structure and electroweak precision constraints, Phys. Rev. D **65**, 055006 (2002).
[15] J. A. Aguilar-Saavedra, R. Benbrik, S. Heinemeyer, and M. Pérez-Victoria, Handbook of vectorlike quarks: Mixing and single production, Phys. Rev. D **88**, 094010 (2013).
[16] A. Banerjee, V. Ellajosyula, and L. Panizzi, Heavy vectorlike quarks decaying to exotic scalars: A case study with triplets, J. High Energy Phys. 01 (2024) 187.
[17] R. Benbrik, M. Berrouj, M. Boukidi, A. Habjia, E. Ghourmin, and L. Rahili, Search for single production of vector-like top partner $T \to H^+ b$ and $H^\pm \to tb^-$ at the LHC Run-III, Phys. Lett. B **843**, 138024 (2023).
[18] Q.-G. Zeng, Y.-S. Pan, and J. Zhang, Search for the signal of vector-like bottom quark at LHeC in the final state with 3 b-jets, Nucl. Phys. **B995**, 116347 (2023).
[19] A. C. Canbay and O. Cakir, Investigating the single production of vectorlike quarks decaying into a top quark and W boson through hadronic channels at the HL-LHC, Phys. Rev. D **108**, 095006 (2023).
[20] A. Belyaev, R. S. Chivukula, B. Fuks, E. H. Simmons, and X. Wang, Vectorlike top quark production via an electroweak dipole moment at a muon collider, Phys. Rev. D **108**, 035016 (2023).
[21] L. Shang and K. Sun, Single vector-like quark X production in the tW channel at high energy pp colliders, Nucl. Phys. **B990**, 116185 (2023).

[22] B. Yang, S. Wang, X. Sima, and L. Shang, Singlet vector-like T quark production in association with Wb at the CLIC, Commun. Theor. Phys. **75**, 035202 (2023).
[23] A. Bhardwaj, T. Mandal, S. Mitra, and C. Neeraj, Roadmap to explore vectorlike quarks decaying to a new scalar or pseudoscalar, Phys. Rev. D **106**, 095014 (2022).
[24] A. Bhardwaj, K. Bhide, T. Mandal, S. Mitra, and C. Neeraj, Discovery prospects of a vectorlike top partner decaying to a singlet boson, Phys. Rev. D **106**, 075024 (2022).
[25] J. Bardhan, T. Mandal, S. Mitra, and C. Neeraj, Machine learning-enhanced search for a vectorlike singlet B quark decaying to a singlet scalar or pseudoscalar, Phys. Rev. D **107**, 115001 (2023).
[26] L. Shang, C. Chen, S. Wang, and B. Yang, Single production of vector-like B quark decaying into bZ at future ep colliders, Nucl. Phys. **B984**, 115977 (2022).
[27] F. F. Freitas, J. a. Gonçalves, A. P. Morais, and R. Pasechnik, Phenomenology at the Large Hadron Collider with deep learning: The case of vector-like quarks decaying to light jets, Eur. Phys. J. C **82**, 826 (2022).
[28] R. Benbrik, M. Boukidi, and S. Moretti, Probing charged Higgs bosons in the 2-Higgs doublet model type-II with vector-like quarks, Phys. Rev. D **109**, 055016 (2024).
[29] G. Corcella, A. Costantini, M. Ghezzi, L. Panizzi, G. M. Pruna, and J. Šalko, Vector-like quarks decaying into singly and doubly charged bosons at LHC, J. High Energy Phys. 10 (2021) 108.
[30] A. Belyaev, R. S. Chivukula, B. Fuks, E. H. Simmons, and X. Wang, Vectorlike top quark production via a chromomagnetic moment at the LHC, Phys. Rev. D **104**, 095024 (2021).
[31] A. Deandrea, T. Flacke, B. Fuks, L. Panizzi, and H.-S. Shao, Single production of vector-like quarks: The effects of large width, interference and NLO corrections, J. High Energy Phys. 08 (2021) 107; 11 (2022) 028(E).
[32] S. Dasgupta, R. Pramanick, and T. S. Ray, Broad toplike vector quarks at LHC and HL-LHC, Phys. Rev. D **105**, 035032 (2022).
[33] S. J. D. King, S. F. King, S. Moretti, and S. J. Rowley, Discovering the origin of Yukawa couplings at the LHC with a singlet Higgs and vector-like quarks, J. High Energy Phys. 05 (2021) 144.
[34] Y.-B. Liu and S. Moretti, Search for single production of a top quark partner via the $T \to th$ and $h \to WW^*$ channels at the LHC, Phys. Rev. D **100**, 015025 (2019).
[35] R. Benbrik *et al.*, Signatures of vector-like top partners decaying into new neutral scalar or pseudoscalar bosons, J. High Energy Phys. 05 (2020) 028.
[36] K.-P. Xie, G. Cacciapaglia, and T. Flacke, Exotic decays of top partners with charge $5/3$: Bounds and opportunities, J. High Energy Phys. 10 (2019) 134.
[37] N. Bizot, G. Cacciapaglia, and T. Flacke, Common exotic decays of top partners, J. High Energy Phys. 06 (2018) 065.
[38] G. Cacciapaglia, A. Carvalho, A. Deandrea, T. Flacke, B. Fuks, D. Majumder, L. Panizzi, and H.-S. Shao, Next-to-leading-order predictions for single vector-like quark production at the LHC, Phys. Lett. B **793**, 206 (2019).
[39] G. Cacciapaglia, A. Deandrea, N. Gaur, D. Harada, Y. Okada, and L. Panizzi, The LHC potential of vector-like quark doublets, J. High Energy Phys. 11 (2018) 055.
[40] A. Carvalho, S. Moretti, D. O'Brien, L. Panizzi, and H. Prager, Single production of vectorlike quarks with large width at the Large Hadron Collider, Phys. Rev. D **98**, 015029 (2018).
[41] A. M. Sirunyan *et al.* (CMS Collaboration), Search for single production of vector-like quarks decaying to a b quark and a Higgs boson, J. High Energy Phys. 06 (2018) 031.
[42] D. Barducci and L. Panizzi, Vector-like quarks coupling discrimination at the LHC and future hadron colliders, J. High Energy Phys. 12 (2017) 057.
[43] A. M. Sirunyan *et al.* (CMS Collaboration), Search for single production of a vector-like T quark decaying to a Z boson and a top quark in proton-proton collisions at $\sqrt{s} = 13$ TeV, Phys. Lett. B **781**, 574 (2018).
[44] C.-H. Chen and T. Nomura, Single production of $X_{\pm 5/3}$ and $Y_{\mp 4/3}$ vectorlike quarks at the LHC, Phys. Rev. D **94**, 035001 (2016).
[45] A. Arhrib, R. Benbrik, S. J. D. King, B. Manaut, S. Moretti, and C. S. Un, Phenomenology of 2HDM with vectorlike quarks, Phys. Rev. D **97**, 095015 (2018).
[46] G. Cacciapaglia, A. Deandrea, N. Gaur, D. Harada, Y. Okada, and L. Panizzi, Interplay of vector-like top partner multiplets in a realistic mixing set-up, J. High Energy Phys. 09 (2015) 012.
[47] A. Angelescu, A. Djouadi, and G. Moreau, Vector-like top/bottom quark partners and Higgs physics at the LHC, Eur. Phys. J. C **76**, 99 (2016).
[48] L. Panizzi, Vector-like quarks: t' and partners, Nuovo Cimento Soc. Ital. Fis. **037C**, 69 (2014).
[49] L. Panizzi, Model-independent analysis of scenarios with vector-like quarks, Acta Phys. Pol. B Proc. Suppl. **7**, 631 (2014).
[50] G. Cacciapaglia, A. Deandrea, L. Panizzi, S. Perries, and V. Sordini, Heavy vector-like quark with charge $5/3$ at the LHC, J. High Energy Phys. 03 (2013) 004.
[51] Y. Okada and L. Panizzi, LHC signatures of vector-like quarks, Adv. High Energy Phys. **2013**, 364936 (2013).
[52] G. Cacciapaglia, A. Deandrea, L. Panizzi, N. Gaur, D. Harada, and Y. Okada, Heavy vector-like top partners at the LHC and flavour constraints, J. High Energy Phys. 03 (2012) 070.
[53] F. del Aguila, L. Ametller, G. L. Kane, and J. Vidal, Vector like fermion and standard Higgs production at hadron colliders, Nucl. Phys. **B334**, 1 (1990).
[54] F. Gianotti *et al.*, Physics potential and experimental challenges of the LHC luminosity upgrade, Eur. Phys. J. C **39**, 293 (2005).
[55] High-Luminosity Large Hadron Collider (HL-LHC): Technical design report V. 0.1, https://cds.cern.ch/record/2749422.
[56] A. Abada *et al.* (FCC Collaboration), HE-LHC: The high-energy Large Hadron Collider: Future circular collider conceptual design report volume 4, Eur. Phys. J. Spec. Top. **228**, 1109 (2019).

[57] A. Abada *et al.* (FCC Collaboration), FCC-hh: The hadron collider: Future circular collider conceptual design report volume 3, Eur. Phys. J. Spec. Top. **228**, 755 (2019).

[58] M. Aaboud *et al.* (ATLAS Collaboration), Search for single production of vector-like quarks decaying into Wb in pp collisions at $\sqrt{s} = 13$ TeV with the ATLAS detector, J. High Energy Phys. 05 (2019) 164.

[59] A. M. Sirunyan *et al.* (CMS Collaboration), Search for single production of vector-like quarks decaying into a b quark and a W boson in proton-proton collisions at $\sqrt{s} = 13$ TeV, Phys. Lett. B **772**, 634 (2017).

[60] ATLAS Collaboration, Search for pair-production of vector-like quarks in lepton + jets final states containing at least one b-jet using the Run 2 data from the ATLAS experiment, http://cds.cern.ch/record/2887901.

[61] J. Cao, L. Meng, L. Shang, S. Wang, and B. Yang, Interpreting the W-mass anomaly in vectorlike quark models, Phys. Rev. D **106**, 055042 (2022).

[62] T. Aaltonen *et al.* (CDF Collaboration), High-precision measurement of the W boson mass with the CDF II detector, Science **376**, 170 (2022).

[63] M. Buchkremer, G. Cacciapaglia, A. Deandrea, and L. Panizzi, Model independent framework for searches of top partners, Nucl. Phys. **B876**, 376 (2013).

[64] V. Cetinkaya, A. Ozansoy, V. Ari, O. M. Ozsimsek, and O. Cakir, Single production of vectorlike Y quarks at the HL-LHC, Nucl. Phys. **B973**, 115580 (2021).

[65] D. Berdine, N. Kauer, and D. Rainwater, Breakdown of the narrow width approximation for new physics, Phys. Rev. Lett. **99**, 111601 (2007).

[66] S. Moretti, D. O'Brien, L. Panizzi, and H. Prager, Production of extra quarks at the Large Hadron Collider beyond the narrow width approximation, Phys. Rev. D **96**, 075035 (2017).

[67] W. F. L. Hollik, Radiative corrections in the standard model and their role for precision tests of the electroweak theory, Fortschr. Phys. **38**, 165 (1990).

[68] M. E. Peskin and T. Takeuchi, New constraint on a strongly interacting Higgs sector, Phys. Rev. Lett. **65**, 964 (1990).

[69] B. Grinstein and M. B. Wise, Operator analysis for precision electroweak physics, Phys. Lett. B **265**, 326 (1991).

[70] M. E. Peskin and T. Takeuchi, Estimation of oblique electroweak corrections, Phys. Rev. D **46**, 381 (1992).

[71] L. Lavoura and J. P. Silva, Oblique corrections from vector-like singlet and doublet quarks, Phys. Rev. D **47**, 2046 (1993).

[72] C. P. Burgess, S. Godfrey, H. Konig, D. London, and I. Maksymyk, A global fit to extended oblique parameters, Phys. Lett. B **326**, 276 (1994).

[73] I. Maksymyk, C. P. Burgess, and D. London, Beyond S, T, and U, Phys. Rev. D **50**, 529 (1994).

[74] G. Cynolter and E. Lendvai, Electroweak precision constraints on vector-like fermions, Eur. Phys. J. C **58**, 463 (2008).

[75] C.-Y. Chen, S. Dawson, and E. Furlan, Vectorlike fermions and Higgs effective field theory revisited, Phys. Rev. D **96**, 015006 (2017).

[76] S.-P. He, Leptoquark and vector-like quark extended model for simultaneous explanation of W boson mass and muon g–2 anomalies*, Chin. Phys. C **47**, 043102 (2023).

[77] A. Arsenault, K. Y. Cingiloglu, and M. Frank, Vacuum stability in the standard model with vectorlike fermions, Phys. Rev. D **107**, 036018 (2023).

[78] R. L. Workman *et al.* (Particle Data Group), Review of particle physics, Prog. Theor. Exp. Phys. **2022**, 083C01 (2022).

[79] M. de Beurs, E. Laenen, M. Vreeswijk, and E. Vryonidou, Effective operators in t-channel single top production and decay, Eur. Phys. J. C **78**, 919 (2018).

[80] N. Kidonakis, Single-top production in the standard model and beyond, in *13th Conference on the Intersections of Particle and Nuclear Physics* (2018), arXiv:1808.02934.

[81] E. Boos and L. Dudko, The single top quark physics, Int. J. Mod. Phys. A **27**, 1230026 (2012).

[82] J. M. Campbell, R. K. Ellis, F. Maltoni, and S. Willenbrock, Production of a W boson and two jets with one b-quark tag, Phys. Rev. D **75**, 054015 (2007).

[83] B. Yang, X. Sima, S. Wang, and L. Shang, Single vectorlike top quark production in the tZ channel at high energy pp colliders, Phys. Rev. D **105**, 096010 (2022).

[84] A. Alloul, N. D. Christensen, C. Degrande, C. Duhr, and B. Fuks, FeynRules 2.0—A complete toolbox for tree-level phenomenology, Comput. Phys. Commun. **185**, 2250 (2014).

[85] J. Alwall, R. Frederix, S. Frixione, V. Hirschi, F. Maltoni, O. Mattelaer, H. S. Shao, T. Stelzer, P. Torrielli, and M. Zaro, The automated computation of tree-level and next-to-leading order differential cross sections, and their matching to parton shower simulations, J. High Energy Phys. 07 (2014) 079.

[86] R. D. Ball *et al.* (NNPDF Collaboration), Parton distributions from high-precision collider data, Eur. Phys. J. C **77**, 663 (2017).

[87] J. Alwall, R. Frederix, S. Frixione, V. Hirschi, F. Maltoni, O. Mattelaer, H. S. Shao, T. Stelzer, P. Torrielli, and M. Zaro, What are the default dynamic factorization and renormalization scales in MadEvent?, https://cp3.irmp.ucl.ac.be/projects/madgraph/wiki/FAQ-General-13 (2011) (accessed on 2023-12-25).

[88] J. de Favereau, C. Delaere, P. Demin, A. Giammanco, V. Lemaître, A. Mertens, and M. Selvaggi (DELPHES 3 Collaboration), DELPHES 3, A modular framework for fast simulation of a generic collider experiment, J. High Energy Phys. 02 (2014) 057.

[89] M. Selvaggi (CERN Collaboration), DELPHES cards for LHC Run-III, HL-LHC and HE-LHC, https://github.com/delphes/delphes/blob/master/cards/delphes_card_HLLHC.tcl (2017) (accessed on 2023-12-25).

[90] M. Selvaggi (CERN Collaboration), DELPHES card for FCC-hh, https://github.com/delphes/delphes/blob/master/cards/FCC/FCChh.tcl (2020) (accessed on 2023-12-25).

[91] M. Cacciari, G. P. Salam, and G. Soyez, FastJet user manual, Eur. Phys. J. C **72**, 1896 (2012).

[92] M. Cacciari and G. P. Salam, Dispelling the N^3 myth for the k_t jet-finder, Phys. Lett. B **641**, 57 (2006).

[93] E. Conte, B. Fuks, and G. Serret, MadAnalysis 5, A user-friendly framework for collider phenomenology, Comput. Phys. Commun. **184**, 222 (2013).

[94] L. Shang and Y. Zhang, EasyScan_HEP: A tool for connecting programs to scan the parameter space of physics models, Comput. Phys. Commun. **296**, 109027 (2024).

[95] G. Cowan, K. Cranmer, E. Gross, and O. Vitells, Asymptotic formulae for likelihood-based tests of new physics, Eur. Phys. J. C **71**, 1554 (2011); **73**, 2501(E) (2013).

[96] N. Kumar and S. P. Martin, Vectorlike leptons at the Large Hadron Collider, Phys. Rev. D **92**, 115018 (2015).